Creating chiral architectures at metal surfaces

2002 J. Phys.: Condens. Matter 14 4119

(http://iopscience.iop.org/0953-8984/14/16/305)

INSTITUTE OF PHYSICS PUBLISHING JOURNAL OF PHYSICS: CONDENSED MATTER

J. Phys.: Condens. Matter **14** (2002) 4119–4132 PII: S0953-8984(02)29075-X

Creating chiral architectures at metal surfaces

R Raval

Leverhulme Centre for Innovative Catalysis and Surface Science Research Centre, Department of Chemistry, University of Liverpool, Liverpool L69 7ZD, UK

E-mail: R.Raval@liv.ac.uk

Received 25 September 2001
Published 11 April 2002
Online at stacks.iop.org/JPhysCM/14/4119

Abstract

The adsorption of complex organic molecules at a metal surface provides a means of introducing the ultimate selectivity function of chirality to a metal surface. Here, the adsorption of *R*, *R*-tartaric acid (*R* standing for rectus), which possesses two chiral centres, on a Cu(110) surface is reviewed. Using a combination of vibrational, surface diffraction, and scanning probe microscopy techniques, a detailed molecular picture of the organic/metal interface has been constructed. This reveals that a number of different phases can be created which vary in terms of the local chemistry and bonding of the organic unit and in terms of the long-range-ordered architectures that are created. Of the various phases created, two possess the special quality of extended chirality, where a truly chiral surface which is non-superimposable on its mirror image, is created. Three constraints are shown to be important for sustaining a single chiral domain across the entire surface: local chirality of the adsorbate, a rigid and defined adsorption geometry, and the presence of anisotropic lateral interactions.

1. Introduction

The organic/metal interface underpins a wide range of technical applications, from coatings, adhesives, sensors, catalysts to optoelectronic devices. In most cases the organic layer serves to provide a more sophisticated activity, passivation, or selectivity function than would have been possible with a bare metal surface. This is particularly true for the selectivity function, which requires the finesse of the organic system to be amalgamated with the robust inorganic substrate. A prime example of this is provided by heterogeneous catalysis, where attempts have been made to bestow the supreme functionality of organic molecules, i.e. chirality, onto naturally achiral metal surfaces [1–5]. Chirality is simply a geometric property which dictates that the mirror transformation of an object is a non-identity operation, i.e. the object and its mirror image are non-superimposable. Clearly for this to hold, the object must not possess any inverse symmetry elements. As a result a chiral object can exist in two distinguishable mirror, or enantiomeric, forms. The property of chirality has profound effects in physics, chemistry, and

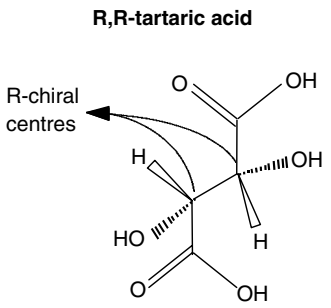

Figure 1. Molecular structure of the *R*, *R*-tartaric acid molecule. The molecule has two chiral centres whose absolute configuration of *R* (for rectus) or *S* (for sinister) are determined by the Cahn–Ingold–Prelog rules [6].

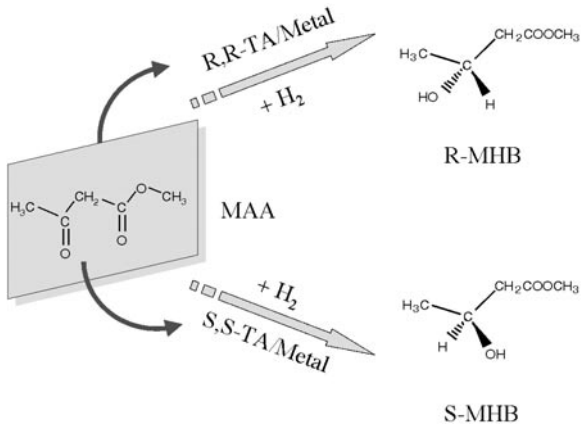

Figure 2. The stereodirected hydrogenation of methylacetoacetate (MAA) to give methyl-3-hydroxybutrate (MHB) on Ni catalysts chirally modified by tartaric acid (TA).

biology, ranging from parity violations for weak forces, to the exclusive use of one mirror form of amino acids by all life-forms on earth. This chirality, or handedness, makes living matter sensitive to the chirality of other materials, often eliciting very different physiological effects to opposite enantiomers. As a result, there is a strong drive to establish enantioselective catalytic methods whereby pure enantiomeric forms of pharmaceuticals, flavours, agrochemicals, etc can be produced. One successful way of creating heterogeneous chiral catalysts [1–5] is to adsorb chiral organic 'modifier' molecules at metal surfaces to introduce asymmetry. For example, the dicarboxylic acid, tartaric acid, which possesses two chiral centres, figure 1, is one of the most successful chiral modifiers. Its presence on Ni and Cu and Co surfaces [2,4,5], endows signification discrimination to the hydrogenation of methylacetoacetate (MAA) to give methyl-3-hydroxybutrate as shown in figure 2. It should be noted that for the bare metal, the probability of hydrogen attack on the planar reactant is identical for each face, yielding a 50:50 racemic product mixture. However, on a nickel surface modified by *R*, *R*-tartaric acid, the reaction is stereodirected, so the *R*-product is produced in $>90\%$ enantiomeric excess. Conversely, modification by *S*, *S*-tartaric acid favours the *S*-product.

In order to gain a fundamental understanding of the nature of the organic/metal interface created in such systems, the behaviour of the modifier *R*, *R*-tartaric acid on a defined Cu(110) surface was investigated. These model modified surfaces were probed using three

main techniques: reflection absorption infrared spectroscopy (RAIRS), low-energy electron diffraction (LEED), and scanning tunnelling microscopy (STM). Each technique provides complementary information on the modified interface, enabling a detailed picture of the interface to be constructed. The high-sensitivity, high-resolution vibrational data obtained by Fourier-transform RAIRS provides direct information on the chemical nature of the adsorbed modifier molecules and their perturbation by the surface, while application of the strict dipole selection rule that operates for the technique allows the orientation of the species to be determined. LEED monitors the long-range two-dimensional periodicity of the adlayer while STM provides information on the local arrangements of the modifier molecules within the domains formed at the surface.

2. Experimental procedure

Experiments were carried out using two separate surface analysis instruments, each with a base pressure of better than 2×10^{-10} mbar. The first chamber was interfaced, via auxiliary optics, with a Mattson 6020 FTIR spectrometer to allow RAIRS experiments to be conducted by the single reflection of IR light, at near-grazing incidence, from the Cu(110) surface. RAIR spectra were recorded throughout a continuous dosing regime as sample single-beam infrared spectra and subsequently ratioed against a reference background single-beam spectrum from the clean Cu(110) surface in order to obtain $\Delta R/R^0$ spectra. A liquid-N_2-cooled HgCdTe detector allowed IR data to be collected over the 4000–800 cm^{-1} region and a polarizer placed in front of the detector ensured that only p-polarized light was detected. All spectra were recorded at 4 cm^{-1} resolution with the coaddition of 256 scans. The chamber was also equipped with LEED, quadrupole mass spectrometry, Auger electron spectroscopy (AES), and sample cleaning facilities. LEED patterns displayed on the phosphor screen in the chamber were captured and digitized by a CCD video camera interfaced to a computer.

STM experiments were carried out in a separate Omicron Vakuumphysik chamber which was also equipped with LEED, AES, and sample cleaning facilities. The STM experiments were carried out by creating the required adlayer by specific exposures of the modifier molecules at the required temperature and then cooling to room temperature to record the data. All STM images were acquired in constant-current mode. Depending on the tolerance of the adlayer to electron beam damage, LEED experiments were conducted before or after the STM experiments, in order to provide a direct correlation between the two sets of data.

Prior to all experiments, the Cu(110) crystal was cleaned by cycles of Ar^+ sputtering and annealing at 600 K. The sample cleanliness and surface order were monitored by AES and LEED, respectively.

Pure enantiomers of tartaric acid (99%) were obtained from Fluka Chemical Company and were used without further purification. The required modifier was contained in a small electrically heated glass tube separated from the main vacuum chamber by a gate valve and differentially pumped by a turbomolecular pump. Before sublimation the modifier sample was pumped for a few hours and outgassed at a temperature of ∼350 K. The modifier was then heated to a temperature of ∼370 K and exposed to the copper crystal. During sublimation the main chamber pressure was $\sim 2 \times 10^{-9}$ mbar, ensuring ultra-clean deposition conditions.

Modifier coverage at the surface is given in terms of fractional monolayers (ML), quoted with respect to the number density of surface metal atoms. The adlayer unit mesh is given in standard matrix notation as follows and quoted in the text as (G_{11} G_{12}, G_{21} G_{22}):

$$\begin{pmatrix} a' \\ b' \end{pmatrix} = \begin{pmatrix} G_{11} & G_{12} \\ G_{21} & G_{22} \end{pmatrix} \begin{pmatrix} a \\ b \end{pmatrix}$$

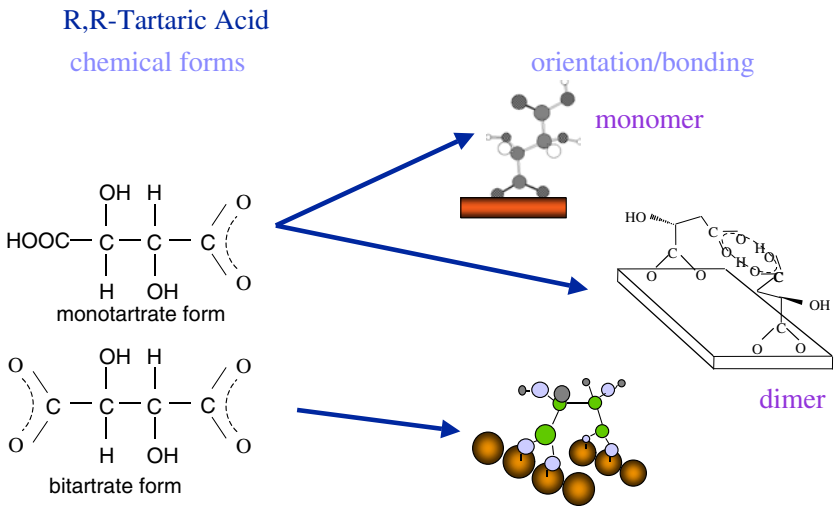

Figure 3. Different local adsorption forms adopted by *R*, *R*-tartaric acid on Cu(110).

where $\boldsymbol{a}'$, $\boldsymbol{b}'$ are the overlayer net vectors and the underlying metal surface mesh is defined by $\boldsymbol{a}$, the unit vector along the $\langle 1\bar{1}0\rangle$ direction, and $\boldsymbol{b}$, the unit vector along the $\langle 001\rangle$ direction.

3. Results and discussion

The adsorption behaviour of *R*, *R*-tartaric acid on Cu(110) under varying coverage and temperature conditions reveals that the modifier/metal system possesses a complex and varied phase space [7–11]. This behaviour arises from a combination of two factors. First, there are dynamic local level changes in the chemical, bonding, and orientational structure that is adopted at a surface, causing the chiral organic molecule to adopt the monotartrate, the bitartrate, or the dimer forms shown in figure 3. Second, these local units display an extraordinary propensity for self-organization at a surface, spawning a series of ordered, crystalline architectures at the surface. As a result, this one simple organic molecule can lead to a multitude of organic/metal interfaces, each possessing different characteristics and functionalities.

Overall, at least six different types of monolayer phase are fashioned in the course of adsorbing *R*, *R*-tartaric acid on Cu(110) [8], depending on adsorption temperature, coverage, and holding time. Of these, only three will be discussed in detail: the (9 0, 1 2) phase which is the preferred low-coverage phase, the (4 0, 2 3) phase which dominates at intermediate coverages, and the (4 1, 2 3) phase that is created at the highest coverages.

3.1. Low-coverage (9 0, 1 2) phase: the bitartrate assembly

The (9 0, 1 2) phase is the thermodynamically preferred phase on Cu(110) at low coverages. However, a significant activation barrier is associated with the creation of this phase [10], and it only forms spontaneously at temperatures in excess of 400 K. Detailed RAIR spectroscopic data for this phase have been discussed elsewhere [8] and reveal that no bands due to the intact COOH acid functionality are present. Instead, bands due to the deprotonated carboxylate COO– functionality are observed, giving rise to characteristic symmetric ν_s(COO) stretching

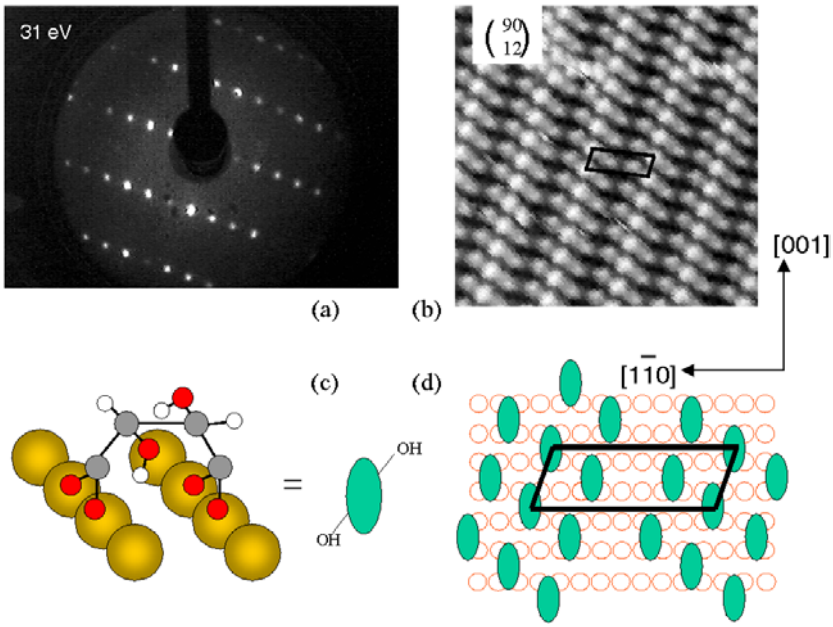

Figure 4. Details of the (9 0, 1 2) chiral phase created at low coverages and high temperatures showing (a) the LEED pattern obtained at 31 eV; (b) a 150 × 200 Å STM image of the chiral surface showing 'trimers' of bitartrate molecules aligned in columns directed along the chiral $\langle 1\bar{1}4\rangle$ direction; (c) the local bonding description of the bitartrate unit; and (d) a schematic model of the overlayer constructed from the STM, LEED, and RAIRS.

vibrations at 1430 and 1410 cm^{-1}. From this, it can be concluded that this adsorbed layer consists entirely of the doubly deprotonated bitartrate species; see figure 2. Application of the RAIRS selection rule also allows one to determine that the two oxygen atoms in each COO unit are held almost equidistant from the surface, thus significantly attenuating the asymmetric ν_{as}(COO) stretching vibration. Both carboxylate ends of the molecule are involved in bonding to the surface, leaving the C2–C3 bond almost parallel to the surface and yielding a fairly rigid adsorption geometry. Following the literature on adsorbed formate [12] and acetate [13], which also bond to the Cu(110) surface via the carboxylate unit, the adsorption site of the bitartrate can be predicted to be one where the oxygens occupy the on-top positions across the two short-bridge sites, figure 4(c). This adsorption site and general geometry have recently been confirmed by periodic density functional theory calculations [14], which also show that the Cu–O bonds have, on average, a length of 1.97 Å.

The two-dimensional nature of this new structure may be constructed from a comprehensive analysis of the LEED and STM data. LEED data—figure 4(a)—reveal that the long-range ordering of modifiers at the surface yields a (9 0, 1 2) structure which is consistent with a very large unit cell possessing the dimensions 23.04 Å × 7.68 Å, $\alpha = 19.47^{\circ}$. High-resolution STM images, displayed in figure 4(b), show that there are three bitartrate molecules per unit cell, resulting in a fractional coverage of $\frac{1}{6}$. The STM images also reveal that rows of three bitartrate molecules assemble at the surface to form long chains, which are aligned along the $\langle 1\bar{1}4\rangle$ surface direction. These growth directions are believed to be dictated by the presence of the α-hydroxy groups attached to both chiral centres of the molecule [9, 14]. We will return to this point in more detail later.

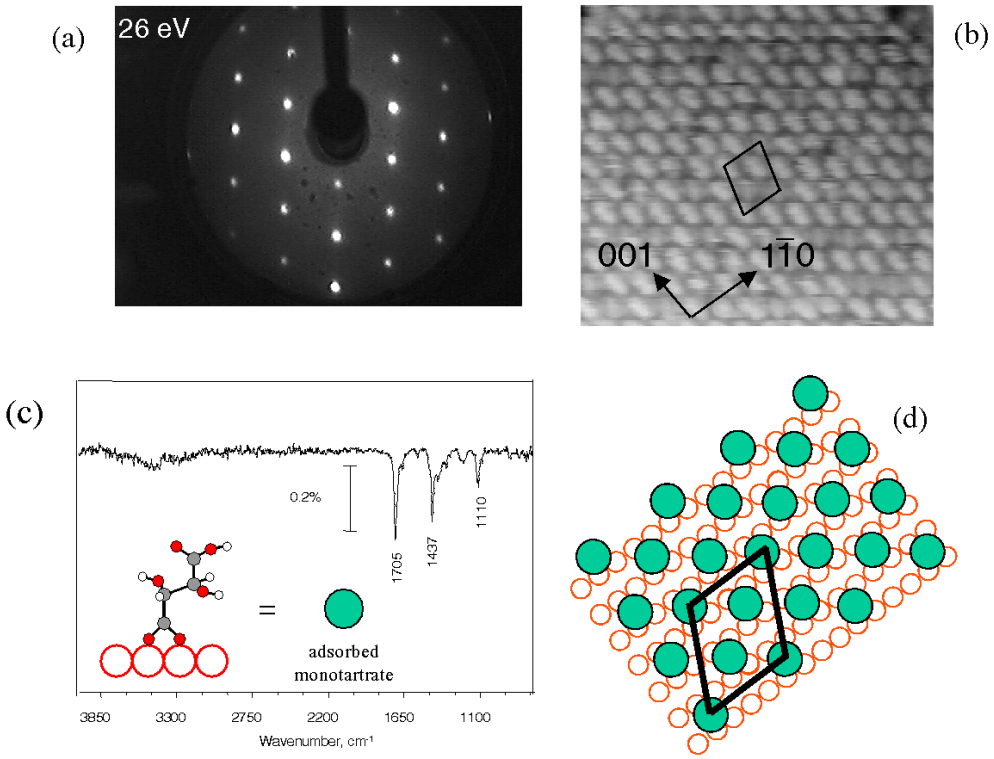

Figure 5. The (4 0, 2 3) phase of *R*, *R*-tartaric acid on Cu(110): (a) the LEED pattern obtained at 26 eV; (b) an STM image (80 × 75 Å; V_{tip}: −1.52 V; I_t: 1.25 nA) showing the position of individual adsorbates; (c) RAIRS data monitoring the nature of the adsorbed species; and (d) a structural model of the phase with the unit cell outlined.

3.2. Medium-coverage (4 0, 2 3) phase: the monotartrate assembly

Although a medium-coverage phase, this structure only presents a low activation barrier for formation and so is created directly as adsorption is carried out on a clean Cu(110) surface at 300 K. STM data show that the nucleation of this phase occurs in the early stages of adsorption and is preferentially located at step edges. Increasing coverage leads to the steady growth of these islands until the entire surface is covered in this phase. Again, detailed information on the nature of this phase has been constructed using a combination of STM, LEED, and RAIRS data. First, LEED photographs of this phase, figure 5(a), show sharp diffraction spots indicating that the islands possess very ordered arrangements of the modifier molecules in a c(4 × 6), or in matrix notation, a (4 0, 2 3) structure, on the Cu surface. This is also a rather large unit cell, but STM data—figure 5(b)—reveal that there are two other molecules within this unit cell, giving a much more packed structure with a local coverage of 0.25 ML.

The chemical detail of the adsorbed entities is provided by RAIR spectra [8] obtained for this phase; see figure 5(c). The presence of both the ν(C=O) vibrations of the acid COOH functionality at 1705 cm^{-1} and the ν_s(COO) vibration of the carboxylate group at 1437 cm^{-1} reveals that the *R*, *R*-tartaric acid is adsorbed as a monotartrate species which is bound to the surface via the deprotonated carboxylate group; see figure 5(c). In addition, the free and intact COOH acid group is held away from the surface and the considerable downshift in frequency

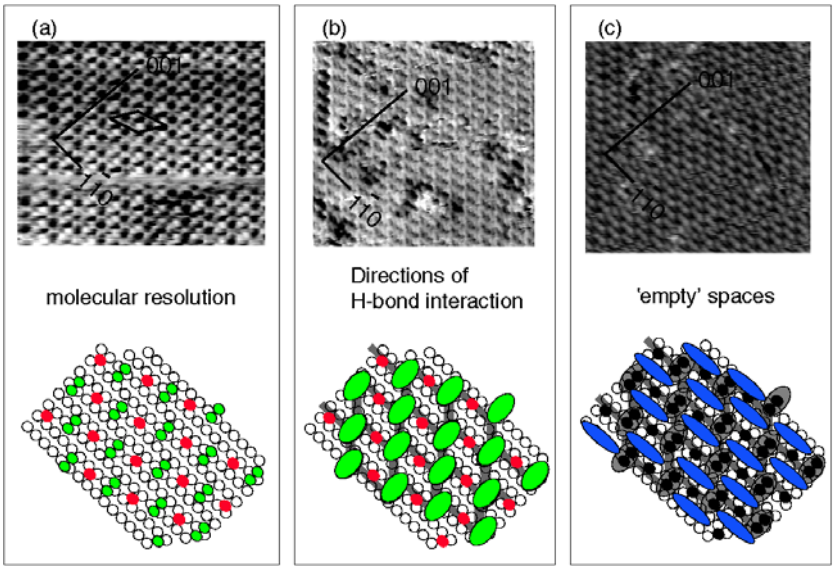

Figure 6. STM images of the (4 1, 2 3) structure taken at different tunnelling conditions. (a) Molecular resolution showing the position of the adsorbed *R*, *R*-TA molecules (150 × 150 Å; V_{tip}: −0.03 V; I_t: 0.51 nA); (b) lines along the $\langle 1\bar{1}2\rangle$ and $\langle 1\bar{1}0\rangle$ directions coinciding with the positions that would have to be adopted by OH groups in order to create a network of H bonds between molecules (150 × 150 Å; V_{tip}: −1.11 V; I_t: 0.46 nA); (c) an inverted image to outline empty spaces in the molecular adlayer (150 × 150 Å; V_{tip}: −1.37 V; I_t: 0.61 nA).

of the ν(C=O) vibration of this group suggests that it is involved in intermolecular H-bonding interactions with the alcohol groups of neighbouring monotartrate species, leading to a strong tendency for island growth in this phase. Combining all these different pieces of information, a fairly complete description of this adsorbed phase is constructed; see figure 5(d).

3.3. High-coverage (4 1, 2 3)phase: the dimer–monomer assembly

Further adsorption beyond a coverage of 0.25 ML leads to the creation of a high-coverage ordered phase at 300 K, which produces a new (4 1, 2 3) LEED pattern. The RAIRS data on this (4 1, 2 3) phase, also discussed in detail elsewhere [8], retain the overall fingerprint of the monotartrate species, but reveal perturbation of the ν(C=O) band which splits into two contributions at 1759 and 1674 cm^{-1}. This is clear indication that two types of COOH acid group now exist in this phase: the latter frequency typical of H-bonded cyclic acid dimers [15, 16] and the former indicative of a monomer or open-chain acid group which involves a lower degree of H bonding. In contrast, the 1437 cm^{-1} vibrational band due to the carboxylate functionality anchored to the Cu(110) remains almost unchanged, indicating that this part of the adlayer is essentially similar to that of the (4 0, 2 3) phases.

STM images of this phase exhibit an ordered and dense adlayer, also with a (4 1, 2 3) repeat structure; see figure 6(a). Using the chemical information above and data from STM images taken at different tunnelling conditions, a model of the (4 1, 2 3) adlayer can be constructed as follows. The STM image in figure 6(a) shows that along the $\langle 001\rangle$ direction, repeat units consisting of a bright two-lobed structure and a smaller feature are seen. The two-lobed structures are held ∼18.0 Å apart along the $\langle 001\rangle$ direction with the smaller feature placed in between. Each two-lobed structure is ∼7.2 Å in length and is observed to stack parallel to

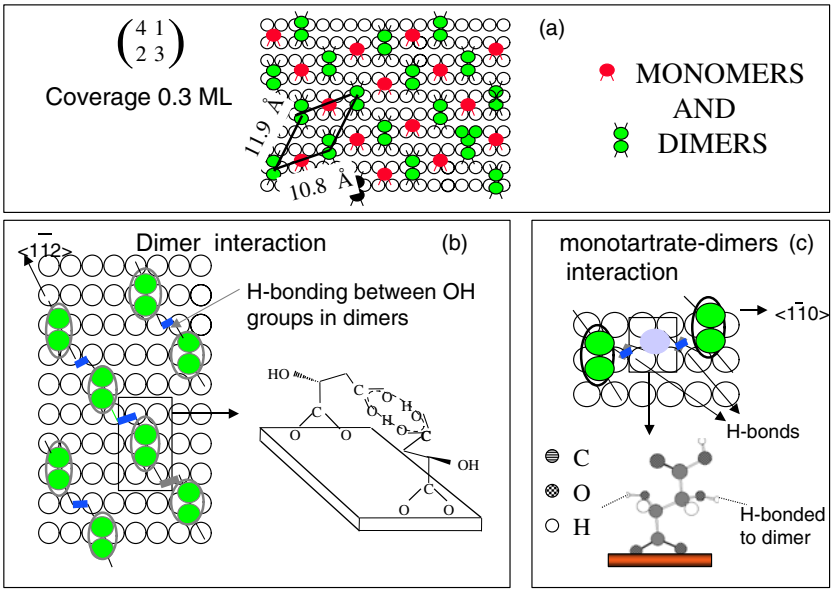

Figure 7. (a) A schematic diagram showing the unit cell and the position of the *R*, *R*-tartaric acid molecules in the (4 1, 2 3) structure; (b) formation of cyclic dimers and hydrogen-bonding interaction between dimers along the $\langle 1\bar{1}2\rangle$ direction; (c) a depiction of single monotartrate molecules involved in further H-bonding interactions along the $\langle 1\bar{1}0\rangle$ direction, thus weaving dimer chains together. Note that in all structures the carboxylate groups bonding with the surface are placed in short-bridged sites, which places each oxygen above a Cu atom.

others in chains along the $\langle 1\bar{1}2\rangle$ direction. The maximum length that a monotartrate molecule can project along the surface is 5 Å, so the two-lobed structure must result from two adsorbed molecules, with the smaller feature arising from a single adsorbed molecule. On this basis, the schematic adlayer in figure 6(d) can be constructed, which clearly possesses the (4 1, 2 3) repeat unit, with a coverage of 0.3 ML. Furthermore, under certain tunnelling conditions, the STM pictures of the (4 1, 2 3) structure show a complex structure interconnected by lines along the $\langle 1\bar{1}2\rangle$ and $\langle 1\bar{1}0\rangle$ axes—figures 6(b) and (e). Finally, figure 6(c) shows an inverted STM image which essentially reveals the 'empty' spaces in the molecular adlayer, depicted in figure 6(f).

The RAIRS data for this structure, which show that cyclic carboxylic acid dimers and monomer acid groups coexist in this structure, allow more chemical detail to be added to the schematic adlayer shown in figure 6(d). It can be seen that the molecules giving rise to the two-lobed STM features are closely placed in this structure and we propose that this proximity leads to the formation of intermolecular cyclic acid dimer units—figure 7(b). In addition, figure 7(b) shows that each cyclic dimer unit possesses two OH groups, one at each end. It can, therefore, be proposed that H-bonding interactions between the OH groups of adjacent dimer units would naturally force the dimer chain along the $\langle 1\bar{1}2\rangle$ direction. We note that the STM image in figure 6(b) also shows strong lines along the $\langle 1\bar{1}2\rangle$ direction, which coincides with the alignments that need to be adopted by these dimer OH groups in order to facilitate strong H-bonding intermolecular interactions. This STM image also shows that similar direct lines are also observed along the $\langle 1\bar{1}0\rangle$ direction, suggesting that the OH groups on the single monotartrate molecules are also involved in H bonding with the adjacent dimer units, tying the entire structure together by connecting neighbouring dimer chains. Here, the coincidence of

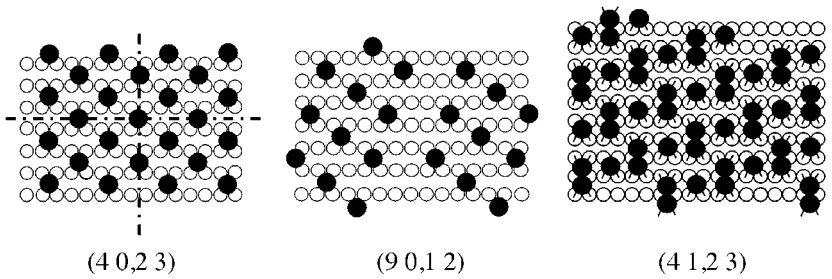

Figure 8. Overall adsorbate templates created by the (4 0, 2 3), the (9 0, 1 2), and the (4 1, 2 3) structures. Whereas the (4 0, 2 3) pattern retains both reflection symmetry planes of the Cu(110) surface, the (9 0, 1 2) and the (4 1, 2 3) pattern do not, thus creating extended chiral surfaces.

the OH groups in the single molecules with the remaining free OH groups of the dimer allows such a H-bonding connection to be easily made along the $\langle 1\bar{1}0\rangle$ direction; see figure 7(c). In such a structure the acid group of the single monotartrate molecules remains free, rationalizing the emergence of the additional ν(C=O) band at 1759 cm^{-1}. The overall pattern adopted by the dimer and monomer adsorbates on Cu(110) is shown in figure 7(a).

4. Manifestations of chirality at the organic/inorganic interface

4.1. The emergence of extended chirality

The discussion on the various phases created by *R*, *R*-tartaric acid on Cu(110) shows that this chiral molecule creates beautiful, crystalline architectures at a surface. We turn now to the question of whether the chiral functionality has been transferred to the interface. Of course, at the trivial level the mere presence of a chiral adsorbate necessarily means that chirality is present locally. However, a close analysis of the phases described above reveals another very interesting phenomenon. If one ignores the local chirality possessed by the molecule and, instead, observes the arrangement of the adsorbates with respect to the surface, it can be seen that the (4 0, 2 3) pattern possesses two reflection symmetry elements but the (9 0, 1 2) and the (4 1, 2 3) templates possess none; see figure 8. Clearly, for the latter two cases, an *extended* chiral surface has been created, which annihilates both reflection symmetry planes of the underlying Cu(110). Importantly, for both phases, the same growth directions and arrangements are maintained over the entire surface and as a result a truly chiral surface is created which is non-superimposable on its mirror image. Whereas local chirality can be easily achieved, the expression for extended chirality is much more difficult to attain and these systems represent some of the first few examples recorded. The constraints that govern the creation of a truly chiral array can be appreciated from figure 9 which shows that the number of allowed space groups rapidly dwindles when going from three-dimensional space (230 space groups) to two-dimensional chiral space groups (only five space groups). Furthermore, it should be noted that when a surface chiral space group is created, it can be expressed in either of its mirror forms—figure 9—which would lead to an overall racemic system. Therefore, it is vitally important that the manifestation of any of the five 2D chiral space groups is strictly restrained so that only one mirror image of the unit mesh is allowed to exist at the surface.

We turn now to the question of what enables the (9 0, 1 2) and (4 1, 2 3) structures to express and sustain true chirality over an entire interface. A consideration of the interface at

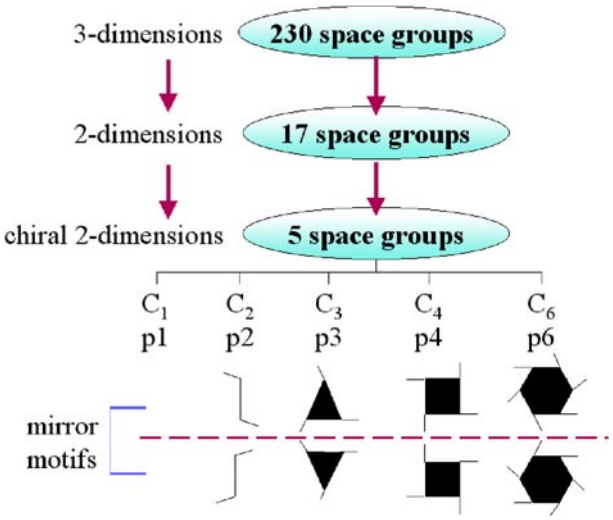

Figure 9. The rapid decrease of allowed space groups going from three dimensions to chiral two dimensions. Each of the five two-dimensional chiral space groups can exist in two mirror motifs. A truly extended chiral surface can tolerate the existence of just one of these two possible motifs.

the molecular level enables the following three conditions to be identified as central to this phenomenon:

- Chirality of the modifier molecule.
- Rigid and defined adsorption geometry.
- Directional and anisotropic lateral interactions.

It can be seen that the (9 0, 1 2) bitartrate and the (4 1, 2 3) dimer phase fulfil all these requirements. The inherent chirality of these molecules and their two-point bonding at the surface uniquely define the 'footprint' the molecule casts at a surface and dictates the position of *all* its functional groups in space. Once this is achieved, the intermolecular interactions between the modifiers control the placement of neighbouring molecules. Here, the chirality of the adsorbates ensures that these lateral interactions are anisotropic. For both cases, we believe that the growth direction is dictated by the spatial positioning of the α-hydroxy groups attached at the chiral centres of the adsorbed species—figures 4 and 7—making the intermolecular interaction uniquely directional. On this basis, a better description of these extended chiral structures is that they are a supramolecular assembly [17] of chiral modifiers. All these factors ensure that only one chiral unit mesh is created and that its mirror twin is never energetically favoured.

4.2. Creating mirror chiral architectures

An important aspect of the asymmetric hydrogenation of β-ketoesters on tartaric acid modified surfaces is that switching the chirality of the modifier switches enantioselectivity from the *R*- to the *S*-reaction product; see figure 2. Therefore, one would expect the mirror enantiomer of the modifier to create a very different surface structure. This can be tested out readily by adsorbing the opposite enantiomer, *S*, *S*-tartaric acid, on Cu(110) and creating the parallel structures. Turning first to the bitartrate structure, a sharp LEED pattern is obtained from the equivalent *S*, *S*-tartaric acid phase, but the positions of the diffraction spots are switched,

consistent with a mirror (9 0, −1 2) structure. This chiral switching is better illustrated by the STM images—figure 10—where the (9 0, −1 2) phase of *S*, *S*-tartaric acid on Cu(110) is revealed to be a true mirror image of the (9 0, 1 2) phase obtained for *R*, *R*-tartaric acid, with every adsorbate position reflected in space [9]. For example, the *S*, *S*-tartaric acid adlayer now shows chain growth in the $\langle\bar{1}14\rangle$ direction and the alignment of molecules in each row of three has also been switched to the mirror orientation. This chiral switching is also observed for the (4 1, 2 3) phase where LEED and STM images—figure 11—show a reversal of all adsorbate positions for the *S*, *S*-tartaric acid system to create the chiral twin surface.

Following on from the discussion in the previous section, this surface chiral switching can be explained in terms of how opposite enantiomers guide the supramolecular assembly directions. For both extended chiral phases created by tartaric acid, the growth direction of the adlayer is dictated by the conformation of the α-hydroxy groups attached to the chiral centres of the adsorbed species. In both structures, the *R*, *R* and *S*, *S* adsorbed species possess defined and rigid adsorption geometries arising from their two-point bonding with the metal surface. As a result they exhibit one major difference, namely the spatial orientation of their OH groups; see figures 10 and 12. Looking down at the surface, it can be seen that the positions of the OH groups on *R*, *R*-tartaric acid in the (9 0, 1 2) structure are oriented in a mirror configuration to those of *S*, *S*-tartaric acid—figure 10. Thus, the enantiomers adopt mirror growth directions, with intermolecular interactions leading to a molecular chain alignment along the $\langle 1\bar{1}4\rangle$ direction for *R*, *R*-tartaric acid, but the mirror $\langle\bar{1}14\rangle$ direction for *S*, *S*-tartaric acid. The same is true for the (4 1, 2 3) phase, where the OH groups connecting the dimer and monomer units occupy mirror positions for the *R*, *R*- and the *S*, *S*-tartaric acid systems, leading to the mirror chiral arrays being created; see figures 11 and 12.

The central role played by the chiral OH groups in guiding supramolecular assembly direction is also nicely illustrated by comparing the (9 0, 1 2) and the (4 1, 2 3) structures; see figures 4 and 7. For the (9 0, 1 2) structures the bitartrate species possesses OH groups along the left-to-right diagonal, while for the cyclic dimer, these groups are now oriented along the right-to-left diagonal. As a result, the assembly directions for the two structures also switch their alignment sense accordingly.

4.3. Sustaining a single rotational domain

The importance of sustaining just one reflection, or mirror, unit mesh in order to create a perfect extended chiral array has been discussed. There is another aspect of the (9 0, 1 2) and the (4 1, 2 3) structures that is also appealing, namely that a single rotational domain is also sustained across the entire surface. Although rotational domains do not threaten the chirality of a system and would not affect the heterogeneous enantioselective response, some optical applications may require the stringent double demand of a single reflection and rotational domain to be maintained across an entire surface. However, adsorption is a random process and initial nucleation events cannot be controlled to occur in only one of many energetically equivalent rotational positions. Generally, rotational domains occur when the overlayer surface mesh possesses a lower symmetry than that of the clean substrate. Therefore, to ensure that all rotational domains that are created are equivalent, rotational symmetry matching of the unit mesh with the surface is needed so that all equally probable adsorption geometries result in an identical nucleation point. It can be seen that this is exactly the case for the (9 0, 1 2) and the (4 1, 2 3) structures—figures 4 and 7. Both possess unit meshes with C_2 point group symmetry, which rotationally matches the twofold axis of the underlying Cu(110) surface.

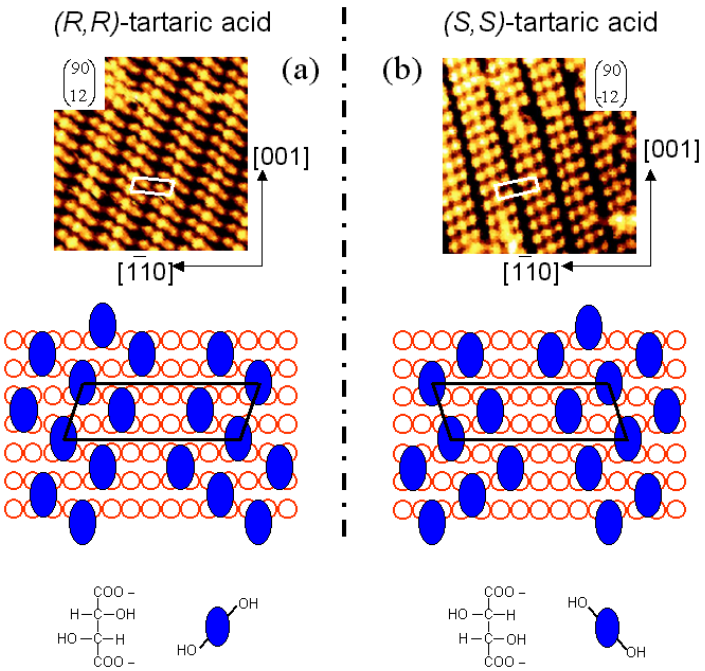

Figure 10. Switching extended surface chirality for the (9 0, 1 2) phase: (a) *R*, *R*-tartaric acid versus (b) *S*, *S*-tartaric acid. This chiral switching is illustrated by the 108 × 108 Å STM images and the schematic models of mirror adlayers created when (a) *R*, *R*-tartaric acid and (b) *S*, *S*-tartaric acid are adsorbed on Cu(110). Note the mirror positioning of the OH groups for (a) the *R*, *R*- and (b) the *S*, *S*-tartaric acid adsorbates.

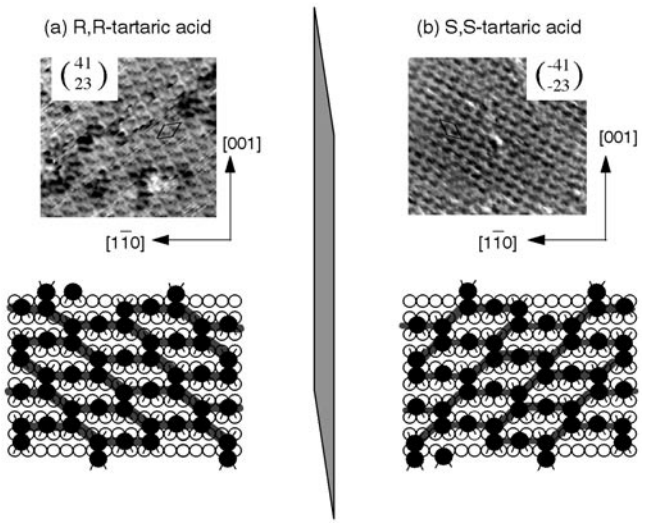

Figure 11. Switching extended surface chirality for the (4 1, 2 3) phase: (a) *R*, *R*-tartaric acid versus (b) *S*, *S*-tartaric acid. This chiral switching is illustrated by the 110 × 100 Å STM images and the schematic models of mirror adlayers created when (a) *R*, *R*-tartaric acid and (b) *S*, *S*-tartaric acid are adsorbed on Cu(110).

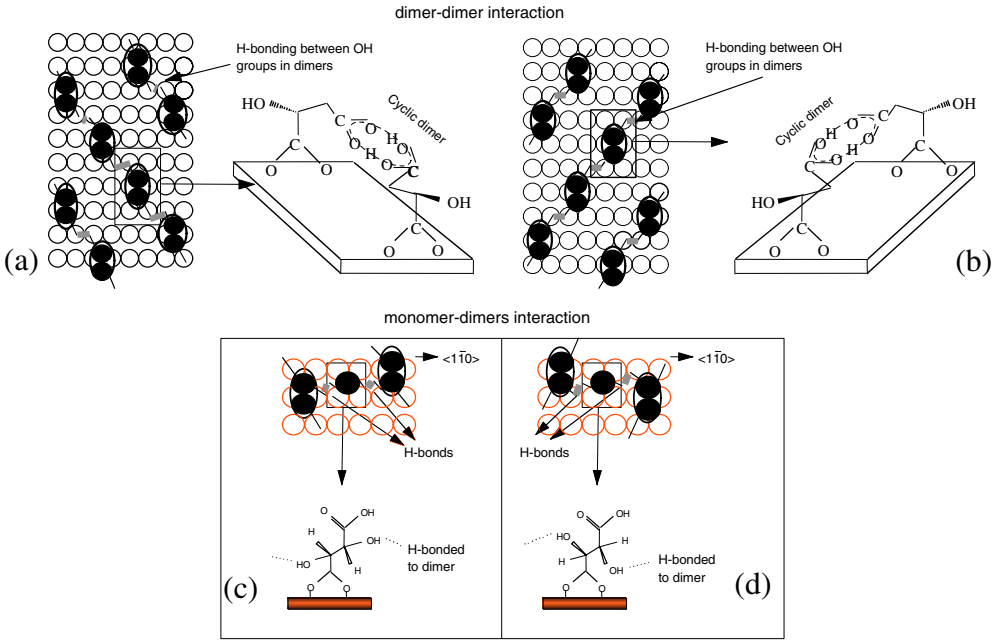

Figure 12. Schematic diagrams to show how the dimer–dimer interaction is switched in direction when going from (a) the *R*, *R*-tartaric acid system to (b) the *S*, *S*-tartaric acid system. The same chiral switching occurs for the monomer–dimer interactions shown for (c) the *R*, *R*-tartaric acid system to (d) the *S*, *S*-tartaric acid system.

5. Conclusions

The adsorption of the chiral molecule, *R*, *R*-tartaric acid, on Cu(110) has been reviewed. The self-assembly of this molecule creates a number of different ordered architectures at the surface. Of these, two phases have been shown to possess true extended chirality, where a unique chiral unit mesh is created at the surface. The combination of a chiral adsorbate with a rigid and defined adsorption geometry ensures that anisotropic lateral interactions govern the assembly of the adlayer. This leads to unique growth directions which guarantee that the mirror twin unit mesh is energetically inequivalent. These lateral interactions are thought to arise directly as the result of the α-hydroxy groups present at the chiral centres of the tartaric acid molecule. Hence, switching chirality of the adsorbate reverses the chirality of the extended surface. Finally, rotational matching of the chiral unit meshes with that of the Cu(110) surface ensures that a single rotational domain is also maintained across the entire surface.

Acknowledgments

It is a great pleasure to acknowledge the substantial contributions that my co-researchers, Maria Ortega Lorenzo, Sam Haq, Chris Baddeley, Chris Muryn and Paul Murray, have made to this research effort. A special thank you also goes to Vincent Humblot for his kind help in preparing a number of the illustrations.

References

[1] Baiker A and Blaser H U 1997 *Handbook of Heterogeneous Catalysis* vol 5, ed G H Ertl, H Knozinger and J Weitkamp (New York: VCH) p 2422
[2] Blaser H U 1991 *Tetrahedron: Asym.* **2** 843
[3] Baiker A 1998 *Curr. Opin. Solid State Mater. Sci.* **3** 86
[4] Izumi Y 1983 *Adv. Catal.* **32** 215
[5] Tai A and Harada T 1986 *Tailored Metal Catalysts* ed Y Iwasawa (Dordrecht: Reidel) p 265
[6] Cahn R S, Ingold C K and Prelog V 1966 *Angew. Chem.* **78** 413
Cahn R S, Ingold C K and Prelog V 1966 *Angew. Chem. Int. Edn* **5** 385
[7] Raval R, Baddeley C J, Haq S, Louafi S, Murray P, Muryn C, Ortega Lorenzo M and Williams J 1999 *Stud. Surf. Sci. Catal.* **122** 11
[8] Ortega Lorenzo M, Haq S, Murray P, Raval R and Baddeley C J 1999 *J. Phys. Chem.* B **103** 10 661
[9] Ortega Lorenzo M, Baddeley C J, Muryn C and Raval R 2000 *Nature* **404** 376
[10] Ortega Lorenzo M, Humblot V, Murray P, Baddeley C J, Haq S and Raval R 2002 *J. Catal.* **205** 123
[11] Raval R 2001 *CATTECH* **5** 12
[12] Woodruff D P, McConville C F and Kilcoyne A L D 1988 *Surf. Sci.* **201** 228
[13] Bao S, Liu G and Woodruff D P 1988 *Surf. Sci.* **203** 89
[14] Barbosa L A M M and Sautet P 2001 *J. Am. Chem. Soc.* **123** 6639
[15] Avram M 1972 *Infrared Spectroscopy—Applications in Organic Chemistry* (New York: Wiley) pp 388–98
[16] Bellamy L J 1964 *The Infrared Spectra of Complex Molecules* (London: Methuen) pp 161–70
[17] Lehn J-M 1995 *Supramolecular Chemistry* (Weinheim: VCH)